Heliyon 7 (2021) e06399

Contents lists available at ScienceDirect

Heliyon

journal homepage: www.cell.com/heliyon

Research article

Fungal and metabolome diversity of the rhizosphere and endosphere of *Phragmites australis* in an AMD-polluted environment

Chimdi Mang Kalu [a,*], Henry Joseph Oduor Ogola [b], Ramganesh Selvarajan [b], Memory Tekere [b], Khayalethu Ntushelo [a]

[a] Department of Agriculture and Animal Health, University of South Africa, Florida Science Campus; Roodepoort, 1709, South Africa
[b] Department of Environmental Science, University of South Africa, Florida Science Campus; Roodepoort, 1709, South Africa

ARTICLE INFO

Keywords:
Rhizosphere
Heavy metals
Phragmites australis
Acid mine drainage
Metallophytes
Phytorhizomediation

ABSTRACT

Symbiotic associations with rhizospheric microbial communities coupled with the production of metabolites are key adaptive mechanisms by metallophytes to overcome metal stress. However, little is known about pseudometallophyte *Phragmites australis* interactions with fungal community despite commonly being applied in wetland phytoremediation of acid mine drainage (AMD). In this study, fungal community diversity and metabolomes production by rhizosphere and root endosphere of *P. australis* growing under three different AMD pollution gradient were analyzed. Our results highlight the following: 1) *Ascomycota* and *Basidiomycota* were dominant phyla, but the diversity and richness of taxa were lower within AMD sites with *Penicillium*, *Candida*, *Saccharomycetales*, *Vishniacozyma*, *Trichoderma*, *Didymellaceae*, and *Cladosporium* being enriched in the root endosphere and rhizosphere in AMD sites than non-AMD site; 2) non-metric multidimensional scaling (NMDS) of 73 metabolomes revealed spatially defined metabolite exudation by distinct root parts (rhizosphere *vs* endosphere) rather than AMD sites, with significant variability occurring within the rhizosphere correlating to pH, TDS, Fe, Cr, Cu and Zn content changes; 3) canonical correspondence analysis (CCA) confirmed specific rhizospheric fungal taxonomic changes are driven by pH, TDS, heavy metals, and stress-related metabolomes produced. This is the first report that gives a snapshot on the complex endophytic and rhizospheric fungal community structure and metabolites perturbations that may be key in the adaptability and metal phytoremediation by *P. australis* under AMD environment.

1. Introduction

In the last century, tremendous global development has been associated with anthropogenic activities that have led to the degradation of soil and water environments. Acid mine drainage (AMD), an outflow of highly acidic and metal-rich water from mineral mining sites, is one of the worldwide problems leading to ecological destruction of watersheds and the contamination of human water sources by inorganic acids, coupled with heavy metals toxicity. Due to stringent federal and state environmental regulations, AMD wastes must be treated before discharge. Therefore, several AMD remediation technologies, mostly focusing on the treatment of already produced AMD before their discharge into water bodies, are currently being applied across the globe [1]. Phytoremediation is one of the emerging technologies for the reclamation of AMD-polluted water and soil environments due to higher costs associated with conventional AMD remediation approach [2].

Under a metalliferous environment, metal tolerant plant species (either obligate/facultative metallophytes or hyperaccumulators) have developed adaptive mechanisms that enable them to survive the elevated metal levels. Stress tolerant and pseudometallophyte *Phragmites australis*, a common perennial rhizomatous and stoloniferous wetland reed frequently used in passive treatment systems of AMD-polluted and other contaminated environments [3, 4, 5, 6], possesses the ability to accumulate more phosphorous and potassium than other macrophytes, in addition to enhancing the removal of excessive nutrient ions including heavy metals in the environment. It has also been reported as a pesticide degrader including organochlorine compounds via peroxidase pathway [7], and removing heavy metals from polluted soils by accumulating them in the roots, stems, and leaves [8, 9, 10]. Under such environment, the symbiotic plant-microbe-metal interactions involving root exudates and microorganisms in rhizosphere ecology play significant role in

* Corresponding author.
E-mail addresses: kaluchimdimang@yahoo.com (C.M. Kalu), ntushk@unisa.ac.za (K. Ntushelo).

https://doi.org/10.1016/j.heliyon.2021.e06399
Received 15 November 2020; Received in revised form 18 February 2021; Accepted 25 February 2021

promoting host adaptation to metal toxicity, phytoremediation and other ecological stress [11, 12].

Generally, plant exudates a cocktail of small and high molecular organic and inorganic molecules in their rhizosphere, creating a nutrient-rich microenvironment that may select for specialized metal-tolerant microorganisms (bacteria and fungi) [13, 14]. In turn, the microbes acting as plant growth promoting microorganisms (PGPMs), may play critical role in adaptation to metal phytotoxicity and stimulate plant growth either indirectly through inducing plant defense mechanisms against phytopathogens, and/or directly through the mineral nutrients solubilization (nitrogen, phosphate, potassium, iron, etc.), production of plant growth promoting substances (e.g., phytohormones), and secretion of specific enzymes (e.g., 1-aminocyclopropane-1-carboxylate deaminase) [11, 12, 15]. For example, *P. australis* has been reported to maintain the carbon-rich rhizosphere through the production of metabolites such as phenols, short-chained organic acids, sugars, and amino acids, that act as an abundant source of energy and nutrients for rhizospheric microbes [10]. Additionally, the reed maintains constant oxygenation of the rhizosphere that enhances the growth of rhizospheric microbiomes that promotes the oxidation of ammonia to nitrate for plant absorption [16], thereby supporting the atmospheric nitrogen cycle. These beneficial interactions help the reed to flourish by colonizing a wide soil volume, quickening photosynthesis, protection from plant pathogens, and enhances their survival in stressed environments. However, such interactions are complex and multifaceted, and thus rhizobiome assembly and the involvement of the *P. australis* in these processes are currently enigmatic. It can be hypothesized that any adverse changes in the environment may result in the corresponding change in the utilization of plant root exudates and the production of stress-induced metabolites that may influence the diversity of metal-tolerant plant growth-promoting rhizospheric and metallophyte-associated endophytic microbial communities. Thus, there has been increased research interest in the last two decades to understand the mechanisms of plant-microbe-metal interactions under stressful environmental conditions that will facilitate wider application of metallophytes in phytorhizomediation.

There is ample evidence that *Phragmites* harbors rich endophytic and epiphytic fungal communities with the potential to play a key role in their adaptability under different environments [17, 18, 19]. According to Dolinar and Gaberščik [20], rhizosphere fungi possess the ability to form living root-soil links, a zone of the soil generally referred to mycorrhizosphere, capable of adjusting the soil properties, microbial networks, or potential root exudates which include metabolites to promote the growth of associated host plant. The role of fungal endophytes in synthesizing defensive compounds and metabolites that enhance the host's survival in stress conditions has also been reported [11, 21]. However, there is a paucity of knowledge on fungal endophytes and ectophytes as well as the community composition of fungi which colonize the rhizosphere of *P. australis*, especially under AMD-polluted environment, despite commonly being applied in wetland remediation of AMD sites. To the best of our knowledge, the impact of the differential production of metabolites in the rhizosphere-root continuum of *P. australis* in AMD environments and its perturbations on rhizospheric fungal community and functional diversity and dynamics has also not been reported elsewhere.

In the present study, we adopted a microcosm-based culture-independent metagenomic and metabolomic approach to gain more knowledge into the nature of in situ microbial community structure and dynamics and primary metabolites production within *P. australis* rhizosphere under AMD-polluted environments. Specifically, the study examined: (1) the community structure and dynamics of rhizospheric soil and endophytic fungi associated with the *P. australis* roots under different AMD-pollution gradient environment; (2) the impact of the AMD pollution gradient on primary metabolites production; (3) the link between fungal community structure, primary metabolites production and the physicochemical characteristics of the AMD environment.

2. Materials and methods

2.1. Study area and sampling

Two sites in Randfontein, Gauteng Province, South Africa., Lan 3 (S 26°07.820, E027°46.680 and elevation of 1693 m), a tailing dam of Mintails Mogale Gold Mine and Wuinze 17 (S 26°07.171, E027°43.305 and elevation of 1670 m), a tailing dam of Sibanye Gold Mine were selected for the study. Florida Lake (S26°10.625, E027°54.220 and 1673 m elevation), a reclaimed recreational (fishing and boat park) freshwater body in the former mining area of Roodepoort, Gauteng, South Africa, was used as a control site (Figure 1). Whereas Florida Lake is characterized by dense and robust growth of *P. australis* on the banks, the two AMD sites had lesser densities of the reed plant, especially at Lan 3 site. All the sites have been in operation for about 20 years. Sampling was conducted under permission from the Johannesburg City Parks and the two mining companies in June 2018.

At each site, we excavated 3 whole plants including the surrounding soils from each of the three quadrats (20 cm × 20 cm) 50 m apart on the shore of the AMD ponds. A total of 9 samples (plants and surrounding rhizospheric soil) were collected in plastic bags and transported on ice (<4 °C) to the laboratory, and root systems immediately processed (by separating the rhizosphere soil and root compartments that forms the root endosphere) within 6 h for metabolites analysis. Fractionation of the rhizosphere soil and the root endosphere was done based on the procedure described by Yamamoto *et al.* [22]. For metagenomic experiments, samples were stored at -80 °C until analysis.

2.2. Physicochemical analysis

Water was scooped with a bucket from each sampling point and physicochemical parameters, namely, pH, salinity, total dissolved solutes (TDS) and electrical conductivity (EC) were measured on-site using Hanna HI9828 multi-parameter ion-specific meter (Hanna Instruments (Pty) Ltd, Bedfordview, South Africa). Rhizospheric soil were initially freeze dried, followed by homogenization by grinding in a pestle and mortar before passing through a 200-mesh sieve. Metal content in mg/L (Fe, Cu, Zn, Mn, Cd, Cr, Co, Na, and Pb), was analyzed in an Inductively Coupled Optical Emission Spectrometer (Agilent Technologies 700 series ICP-OES), following acid microwave digestion of 0.5 g of the soil samples as described previously [23]. One-way analysis of variance (ANOVA) and Tukey's Honest post hoc test ($p < 0.05$) was done using SAS version 9.4 (SAS Institute, Cary, NC, USA) to compare the differences in metal contents among the sampling sites.

2.3. DNA extraction, PCR amplification, and MiSeq high-throughput sequencing

Root endosphere samples were ground into fine particles suitable for DNA extraction. Fecal/Soil Total DNA™ extraction kit (Zymo Research Corporation, CA, USA) was used to extract total DNA from 0.25 g of rhizosphere soil or ground root samples according to manufacturer's protocol. The quantity and the quality of the resultant environmental DNA was checked on a 1.5% agarose gel and Biodrop μLite spectrophotometer (Biochrom Ltd, Cambridge, UK). Extracted DNA used for downstream PCR and sequencing analysis had A_{260}:A_{280} ratios between 1.8–2.0 and DNA concentrations of 20–150 ng/μL. Equimolar concentration (5 ng) of the environmental DNA of a replicate sample type (endospheric or rhizospheric) for each site were pooled together (9 replicates) to get a representative sample for downstream library preparation.

Libraries of nuclear ribosomal ITS region were amplified from each resultant pooled DNA products using ITS1 (5′-CTTG G TCAT TTAG AGGA AGTA ACCT ACGG GNGG CWGCAG-3′) and ITS4 (5′-TCCTCCGC TTATTGAT ATGCGGAC TACH VGGG TWTCTAAT-3) primers fused with Illumina MiSeq adapters and barcode sequence (underlined) unique to

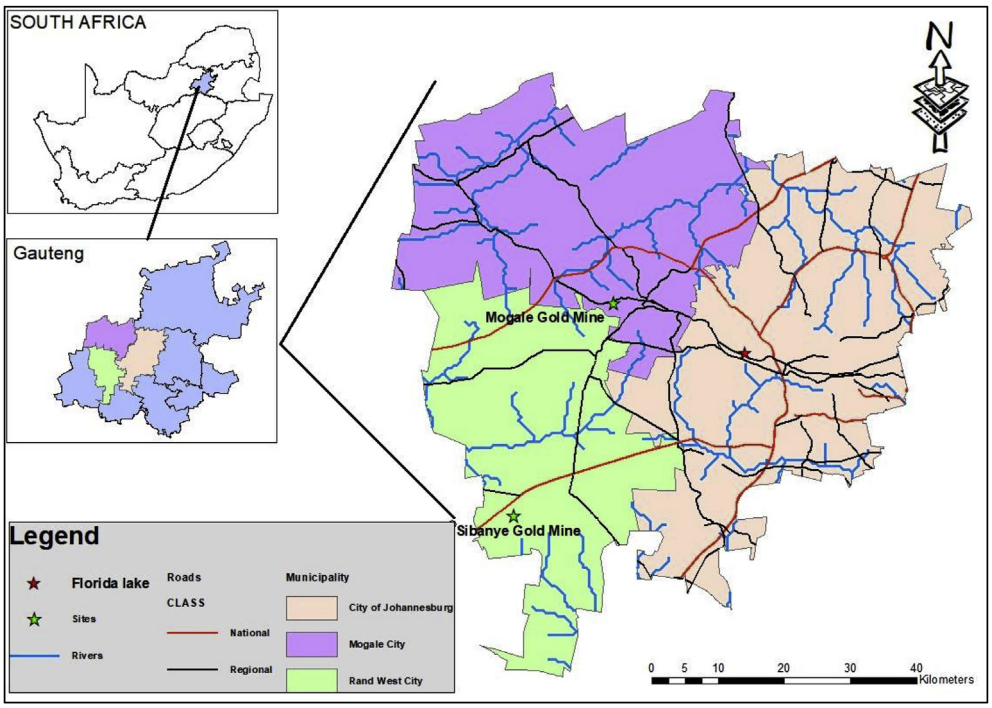

Figure 1. Map showing the sampling sites (Mogale Gold Mine, Sibanye Gold Mine and Florida Lake).

each sample according to MiSeq standard protocol (https://support.illumina.com/documents/documentation/chemistry_documentation/16s/16s-metagenomic-library-prep-guide-15044223-b.pdf). The resultant amplified DNA were cleaned and sequenced by paired-end (300 bp reads each) sequencing on the Illumina MiSeq Platform at Inqaba Biotechnology (Pretoria, South Africa).

2.4. Data processing and ITS gene-based community analysis

The obtained Fastq datasets were initially scrutinized for PCR artefacts and low-quality reads (reads with >50% bases having a quality score < 2) using ngsShoRT (next generation sequencing short reads) trimmer as described by Chen *et al.* [24]. The merging of the forward and reverse sequences was done following the protocols of Magoč *et al.* [25]. The resultant sequences were further strictly filtered to remove low quality sequences as described by Bokulich *et al.* [26], before being subjected to QIIME pipeline (V2.0, https://qiime2.org/) [27]. According to the method described by Edgar [28], chimeric sequences were removed, and the sequence clustered into operational taxonomic units (OTU) at 97% sequence similarity [29]. Finally, the effective sequence was assigned to representative microbial taxa using the RDP (Ribosomal Database Project) classifier [30].

Alpha diversity indices of Chao1, Shannon, Simpson, evenness, Fisher alpha dominance and Good's coverage were calculated at the genetic distance of 0.03 using the plot richness function of *phyloseq* package in R [31] to reflect the diversity and richness of the fungal community in different samples. The dominant OTUs at different taxonomic levels were used to generate heatmap using *ampvis2* packagein R [32], respectively, to visualize the variations and distributions of present fungal communities. β-diversity based Bray-Curtis dissimilarity distance and canonical correspondence analysis (CCA) to visualize the community relationships between and within each AMD environments with explanatory environmental variables was also performed using Paleontological statistics software package Version 4 (PAST4) [33]. OTU counts were used as "species" data, while AMD site physicochemical data were included in the analysis as "environmental" variables. The most significant variables were initially picked by forward selection at $p < 0.01$ baseline before being included in the final model whose significance was tested with 999 permutations.

2.5. Metabolome analysis

For metabolite extraction, 10 g freshly collected rhizosphere soil and root samples were ground before mixing with 1 ml 75%:25% v/v methanol: water solution. The mixture was vortexed briefly, then sonicated for 10 min and centrifuged at 13,000 rpm for 5 min. The supernatant was then filtered with a 0.22 μm Whatman filter membrane and transferred into vials. Then, the samples were directly analyzed to determine their metabolomic profiles including organic acids, vitamins, and signaling molecules using LCMS-8040 triple quadrupole mass spectrometer (Shimadzu Corporation, Kyoto, Japan), equipped with Shimpack Velox® PFPP (pentafluorophenylpropyl) column (Shimadzu Corporation, Kyoto, Japan). The instrument settings for the LCMS/MS were as follows; total flow = 0.4 mL/min, injection volume = 1 μl, oven temperature = 40 °C/max 85 °C, nebulizing gas flow = 3 L/min, drying gas flow = 15 L/min and the mobile phase was 50%/50% acetonitrile/water. Peak detection, data mining, alignment and normalization, removal of isotope masses, and library searching was performed using LabSolutions Insight® multi-analyte quantitation software (Shimadzu Corporation, Kyoto, Japan).

To compare the peak abundance of molecular features, peak area values were exported from LabSolutions Insight® to Microsoft Excel. The major metabolites peak areas were used to generate stacked bar charts and heatmap using *ggplot2* [34] and *heatmap.2* packages [35] in R, respectively, to visualize the variations and distributions of present metabolites in the rhizospheric soil and roots samples. Using metaMDS and anosim function of the *vegan* package in R [36], non-metric multidimensional scaling (NMDS) and ANOSIM, respectively, was calculated to explore the metabolite data structure based on dissimilarity measurement (Bray-Curtis dissimilarity) between three AMD environments and localization (rhizosphere versus endosphere). The NMDS plots were generated using *ggplot2* package in R. When the ANOSIM analysis suggested significant differences in metabolome structure between groups, we then determined which metabolites were driving those differences by

identifying indicator species (metabolites) using the R package *indicspecies* [37]. This analysis generates an indicator value (*IndVal.g*) that measures the association between OTUs with each group or combination of groups and then identifies the group corresponding to the highest association value. In this study, indicator metabolites based on an IndVal of >0.30 and a $p < 0.05$ assessed after 999 permutation tests.

2.6. Data availability

All the data analysis results obtained during this study are included in the manuscript (and its Supplementary 36 Information files). All the raw datasets from Illumina sequencing have been deposited at the NCBI database (https://www.ncbi.nlm.nih.gov/) sequence archive (SRA) as BioProject ID PRJNA640287.

3. Results

3.1. Physicochemical profiles of AMD samples

Physicochemical parameters of the three sampling sites (two acid mine sites (Lan 3 and Wuinze 17) and the control site (Florida Lake)) showed significant differences for each of the parameters measured (Table 1). The acid mine sites had significantly ($p < 0.05$) higher EC, salinity, TDS, and low pH when compared to the non-AMD control site (Table 1). Further, the heavy metal analysis also showed significantly higher ($p < 0.05$) values in the AMD sites rhizospheric soil samples, that were >5-fold higher, than the values for the non-AMD control site, especially with Fe, Na, Cr, and Zn (Table 1).

3.2. Root endosphere and rhizosphere fungal community diversity and distribution under different AMD pollution

3.2.1. Diversity analysis of fungal communities

Fungal diversity analysis based on the nuclear ribosomal ITS region analysis resulted in 382,391 quality reads and 707 OTUs across six samples (Table 2). Good's coverage across the sample was >98%, implying that the sampling deepness was enough to estimate the diversity enclosing all major fungal groups inhabiting the studied root endosphere and rhizosphere of *P. australis* under the different AMD environments (Table 2). This was further supported by the rarefaction curves (Figure 2a) and rank abundance plot (Supplementary Information Figure 1) that asymptotically approached a plateau, suggesting that the curves accurately reflected the fungal community.

According to observed OTU numbers, the sample FL_A (154) had the richest diversity, followed by FL_E (122), Wuinze17_A (119), and Lan3_A that had comparable moderate diversities, whereas rhizosphere samples Wuinze17_A (114) and Lan3_E (90) had less richness. Similarly, the calculated alpha diversity indices (dominance, Chao1 index, Shannon index, Simpson's index, and evenness) showed that FL samples (both rhizosphere and root endosphere) had more representation and evenness of the taxa than other sites (Table 2). All the biodiversity indices separated the acid mine sites (Lan 3 and Wuinze 17) from the non-acid mine site (Florida Lake). The shared fraction of core fungal OTUs associated with the rhizosphere and root endosphere is summarized in Figure 2b. Based on the Venn diagram analysis, 70 and 63 OTUs constituted the core microbiota in the rhizosphere and root endosphere, respectively, accounting for ~99% of the total abundances. In the rhizosphere, 20 OTUs (78.7% abundance) were common in all the three AMD sites, with 3 OTUs shared between Lan 3 and Wuinze 17, 5 OTUs between Florida Lake and Lan 3, and 6 OTUs between Florida and Wuinze 17.

3.2.2. Taxonomic composition of the AMD environment fungal communities

Based on relative abundances, fungal groups in the different *P. australis* root endosphere and rhizosphere grouped into 8 phyla, 28 classes, 84 orders, and 259 genera. Figure 3 summarizes the abundance of the fungal community at phylum, class, and genera level. Overall, members of phylum *Ascomycota* and *Basidiomycota* were the most abundant across all the sampling sites, accounting for >75% of the observed taxa (Figure 3a). Approximately 1–20% of the sequences were unidentified even to a phylum level with the BLAST-based classifications employed, with most unclassified fungi observed in the non-AMD site rhizosphere (FL_E, 20%) and AMD site root endosphere (Lan E, 18.5%). However, subtle variations in classified fungal taxa within and between sampling sites were discernible. Florida Lake site was characterized by a higher abundance of phylum *Basidiomycota*, accounting for 40% and 90% of taxa in the rhizosphere and root endosphere, respectively. In contrast, *Ascomycota* constituted the major phylum in AMD sites, accounting for ~90% and 70% abundance of taxa in the rhizosphere and root endosphere, respectively. The other minor phyla (<1% relative abundances) identified included *Entorrhizomycota*, *Glomeromycota*, *Monoblepharomycota*, *Mucoromycota*, and *Rozellomycota*. At the class level, *Eurotiomycetes*, *Saccharomycetes*, *Tremellomycetes*, *Agraricomycetes*, *Microbotryomycetes*, *Ustlaginomycetes*, *Dothideomycetes*, *Sordariomycetes*, *Leotiomycetes*, and *Cystobasidiomycetes* were the abundant classes with variation in their abundance across the sampling sites (Figure 3b).

The relative abundance of the fungal communities at the genera level (Figure 3c) also provided more insight into the taxonomic differences between the rhizosphere and root endosphere of *P. australis* in AMD and the control site. In the rhizosphere samples, the two AMD sites clustered together separating them from the genera found in the non-AMD site. The most abundant genera occurring in the two sites included *Aspergillus*, *Penicillium*, *Candida* and unclassified *Saccharomycetales*. In the root

Table 1. Summary of the mean (±SD) physicochemical variables water and heavy metal content of the rhizospheric soil of *P. australis* growing in two acid mine sites (Lan 3 and Wuinze 17) and non-acid mine site (Florida Lake) (n = 9).

Variables	Lan 3	Wuinze 17	Florida Lake
EC (μS/cm)	5537 ± 2.7^{a}	2180 ± 1.2^{b}	113 ± 0.1^{c}
TDS (mg/L)	4305 ± 1.6^{a}	1295 ± 0.8^{b}	102 ± 0.4^{c}
Salinity (g/kg)	3.20 ± 0.3^{a}	1.26 ± 0.11^{b}	0.10 ± 0.002^{c}
pH	5.01 ± 0.27^{c}	6.50 ± 0.6^{b}	7.81 ± 0.2^{a}
Fe (mg/L)	193.6 ± 7.89^{a}	54.21 ± 6.67^{b}	25.24 ± 1.64^{c}
Cd (mg/L)	0.02 ± 0.001^{a}	0.02 ± 0.003^{a}	0.02 ± 0.001^{a}
Co (mg/L)	0.17 ± 0.02^{a}	0.09 ± 0.01^{b}	0.03 ± 0.003^{c}
Cr (mg/L)	0.39 ± 0.09^{a}	0.05 ± 0.004^{b}	0.01 ± 0.006^{c}
Cu (mg/L)	0.27 ± 0.05^{a}	0.13 ± 0.002^{b}	0.03 ± 0.002^{c}
Na (mg/L)	1.29 ± 0.10^{a}	0.40 ± 0.03^{b}	0.26 ± 0.02^{c}
Pb (mg/L)	0.10 ± 0.02^{a}	0.04 ± 0.005^{b}	0.06 ± 0.005^{c}
Zn (mg/L)	0.50 ± 0.05^{a}	0.21 ± 0.02^{b}	0.11 ± 0.02^{c}

Means with similar small letters (a-c) within a row are not significantly different ($p < 0.05$). EC-electrical conductivity, TDS-total dissolved solute.

Table 2. Summary of sequencing outputs and diversity indices for rhizosphere and root endosphere fungal communities associated with the roots of *Phragmites australis* growing in two acid mine sites (Lan 3 and Wuinze 17) and non-acid mine site (Florida Lake-FL).

Indices	Rhizosphere			Root endosphere		
	Lan3_E	Wuinze17_E	FL_E	Lan3_A	Wuinze17_A	FL_A
Observed OTU	90	110	122	114	119	154
Quality reads	58 217	106 724	25 248	96 400	46 416	49 386
Dominance_D	0.181	0.135	0.080	0.112	0.135	0.099
Simpson_1-D	0.819	0.865	0.920	0.888	0.865	0.901
Shannon_H	2.292	2.538	3.059	2.641	2.753	2.756
Evenness_eH/S	0.110	0.115	0.175	0.123	0.132	0.102
Fisher_alpha	10.43	12.11	16.66	12.77	14.78	19.67
Chao-1	92.63	113.5	132.9	116.1	123.1	156.2
Good's coverage (%)	99.5	99.9	98.9	99.9	99.3	99.8

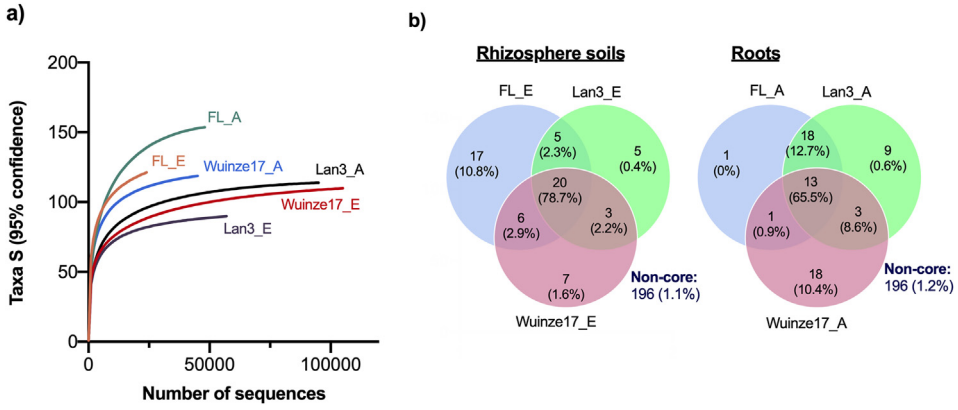

Figure 2. (a) Rarefaction analysis showing the sequence coverage. (b) Venn diagram showing number of OTUs at each location and the shared fraction of core fungal microbiome associated with rhizosphere and root endosphere of *Phragmites australis* growing under AMD environments.

endosphere, despite no clear clustering between the AMD and non-AMD sites, the most abundant taxa were genus *Vishniacozyma*, *Aspergillus*, *Penicillium,* unclassified *Capnodiales*, and *Saccharomycetales*. Core microbiome analysis demonstrated that unique OTUs differed within the sites and between rhizosphere and endosphere (Supplementary Information Table 1). In root endosphere, non-AMD site (FL) had highest number of unique taxa (18 OTUs) while AMD sites had 9 and 1 OTU for Wuinze17 and Lan3_E, respectively. In contrast, 17, 5 and 7 unique OTUs was observed in the rhizospheric samples of FL, Wuinze17 and Lan3, respectively.

3.3. Metabolome profiling

A total of 73 metabolites were annotated based on matching retention time and mass spectra to the in-built LabSolutions Insight® platform database. The metabolites included amino acids (22), nucleotide/nucleosides (17), carbohydrates (9), organic acids (7), vitamins (2), and other known plant metabolites (16) (Supplementary Information Table 2). Figure 4 presents the heatmap showing both the hierarchical clustering analysis (HCA) and relative spectral abundance of the 73 metabolites detected in both rhizosphere and endosphere compartments of *P. australis* roots impacted by different AMD environment. The presented dendrogram indicates sub-clusters containing different primary metabolites with varying degrees of similarities.

Overall, metabolites of the rhizosphere from the two AMD sites (Lan 3 and Wuinze 17) clustered together indicating the closeness of the metabolite profiles in the two sites, but with subtle variation in their spectral abundances (Figure 4). Interestingly, choline was relatively high in all three rhizosphere soil samples. In the root samples, however, clustering was not observed between the two AMD sites but only between an acid mine site (Lan 3) and a control site (Florida Lake).

Beta diversity statistical analyses were also done to determine the statistical significance of spatial heterogeneity in the relative spectral abundance of metabolites. The NMDS plots revealed that samples clustered more by type (whether rhizosphere or root endosphere) (ANOSIM, (R = 0.8567, p < 0.001) rather than by AMD sites (ANOSIM, R = -0.1381, p = 0.9890) (Figure 5). The stress of the NMDS ordination was 0.103. Similarly, goodness of fit analysis also revealed that localization (rhizosphere vs root endosphere) (r^2 = 0.712, p = 0.006) had a significant correlation with metabolites composition compared to habitat (AMD sites) that had a poor and non-significant correlation (r^2 = 0.149, p = 0.934). However, closer inspection of the data showed that variability in primary metabolites was more significant in the rhizosphere than the root endosphere, with rhizospheric samples of AMD sites (Wuinze17 and Lan3) clustering closer together than non-AMD site (Florida Lake) (Figure 5). The study also investigated the effects of physiochemical parameters on metabolites composition and abundance in the rhizospheric samples. To achieve this, the direction and length of the vectors of metabolites and geochemical factors (pH, salinity, TDS, EC and heavy metal content) were computed by Bray-Curtis distances using the "envfit()" function in the *vegan* package [36]. Multicollinearity between variables was tested using Spearman's rank correlation and variables having high correlation (Spearman's ρ^2 > 0.70) were excluded, leading to retention of pH (r^2 = 0.223, p = 0.006), TDS (r^2 = 0.467, p = 0.012), Cr (r^2 = 0.301, p = 0.026), Cu (r^2 = 0.197, p = 0.042), Fe (r^2 = 0.349, p = 0.001), and Zn (r^2 = 0.136, p = 0.039), as the main physicochemical variables influencing the metabolite variability. Vector-fitting of the significant environmental variables to the NMDS ordination space as defined by the metabolite composition is illustrated in Figure 5.

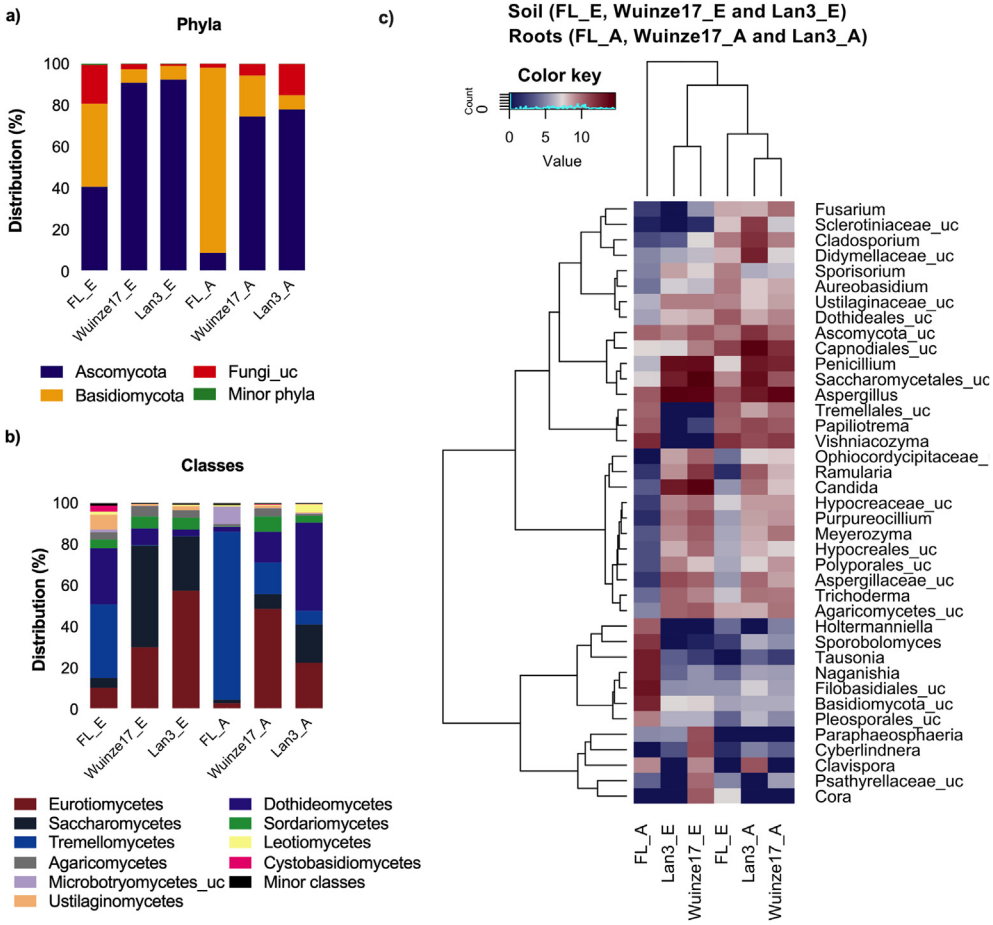

Figure 3. The composition and relative abundance of major fungal taxa associated rhizosphere and the root endosphere of *Phragmites australis* growing in different AMD polluted environments. (a, b) Stacked plots of the relative abundance at top phyla and class level (>1% abundance). (c) Heatmap of log_2 normalized counts of the 40 most abundant genera. The dendrogram shows complete-linkage agglomerative clustering based on a Euclidean distance. The heatmap color (blue to reddish-brown) represent the row z-score of the mean relative abundance from low to high.

To identify differentially abundant metabolites between different groups (rhizosphere *vs* root endosphere), a metabolite-group association analysis using the multipatt function of the "*indicspecies*" R package [37] was performed. As shown in Table 3, nine metabolites (adenosine, acetylcholine, symmetric dimethylarginine, asymmetric dimethylarginine, dopa, guanosine monophosphate, kynurenine, isoleucine, and leucine) were significantly ($p < 0.05$) associated with the root endosphere. In contrast, niacinamide, creatinine, ophthalmic acid, 2-ketoglutaric acid, serotonin, histamine, guanosine, methionine, dimethylglycine, thymidine monophosphate, thymine, choline, cystathionine, proline, and valine were significantly associated with the rhizosphere ($p < 0.05$).

3.4. Relationship between fungal community, primary metabolites, and physicochemical parameters

To examine which of the physicochemical parameters and primary metabolomes in both root endosphere and rhizosphere were most likely associated with variation of the fungal community, the study explored their relationship in a multivariate canonical correspondence analysis (CCA) (Figure 6). The CCA triplot showed that the concentration of metabolites (dimethylglycine, ophthalmic acid, histamine, serotonin, 2-ketoglutaric acid, thymidine monophosphate, proline, and choline), were positively and significantly ($p < 0.01$, after Bonferroni correction) associated with rhizospheric microbiomes (mainly *Saccharomycetales* and *Agaricales*) of Wuinze 17, while pH, TDS, Cr, Fe, Zn and metabolites (methionine, valine, creatinine, thymine, niacinamide, and cystathionine) were related to Lan 3 rhizospheric microbiomes such as *Polyporales*, *Eurotiales*, *Hypocreales*, *Agaricomycetes_uc*, and *Basidiomycota_uc* (Figure 6a). In Florida Lake's rhizosphere sample, pH was the major physicochemical parameter that influenced the fungal community and it showed a strong positive correlation with fungi belonging to the genera *Ascomycota_uc*, *Capnodiales*, *Cystofilobasidiales*, and *Sporodiabolales*. In contrast, pH negatively correlated ($p < 0.01$) to rhizosphere microbiome diversity in Lan_3. The result showed that the AMD sites induced the production of more primary metabolites by the reed but selected for fewer associated fungi.

Inferences from the CCA analysis also showed that a correlation exists between the fungal community in the root endosphere of *P. australis* and the primary metabolites (Figure 6b). The fungal community at the order level and primary metabolites showed close ordination indicating the impact of AMD pollution on the metabolites produced by the root tissues and the diversity of endophytic fungi. Fungal taxa such as *Ascomycota_uc*, *Capnodiales*, and *Saccharomycetales* showed a strong positive correlation with kynurenine, acetylcholine, and dopa in Lan 3, whereas *Eurotiales*, *Hypocreales*, *Ustilaginales*, and *Dothideales* positively correlated with adenosine, asymmetric dimethylarginine, symmetrical dimethylarginine, and leucine in Wuinze 17. In contrast, orders belonging to phylum *Basidiomycota* such as *Filobasidiales*, *Sporidiobolales*, *Holtermannlales*, and *Tremellales* in Florida Lake showed a strong positive correlation with guanosine monophosphate and isoleucine.

4. Discussion

4.1. Rhizosphere and endosphere fungal community of P. australis under AMD conditions

This study describes the diversity of rhizospheric fungal communities associated with AMD heavy metal pollution gradient and plant root exudate profile. Overall, the results showed that the diversity and richness of the fungal community in both the root endosphere and rhizosphere in *P. australis* growing under the non-AMD control site were higher than in the

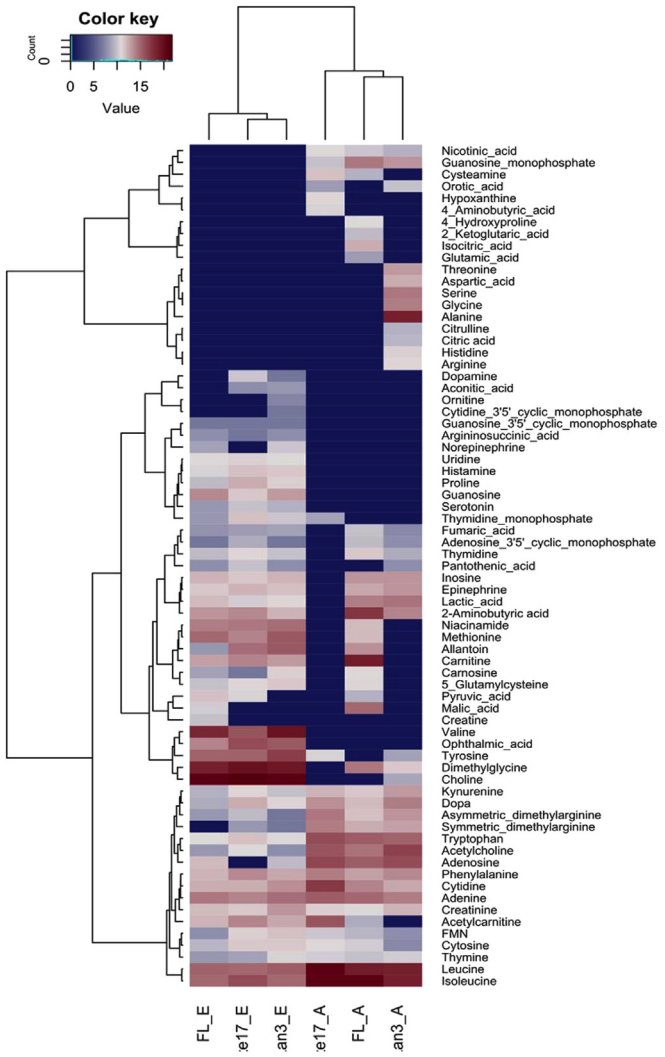

Figure 4. Hierarchical clustering analysis of different primary metabolites present in the rhizosphere soil (FL_E, Wuinze17_E and Lan3_E) and roots samples (FL_A, Wuinze17_A and Lan3_A) of *Phragmites australis*. Heatmap was generated from log2 normalized spectral abundance. The dendrogram shows complete-linkage agglomerative clustering based on a Euclidean distance. The heatmap color (blue to reddish-brown) represent the row z-score of the mean relative abundance from low to high, respectively.

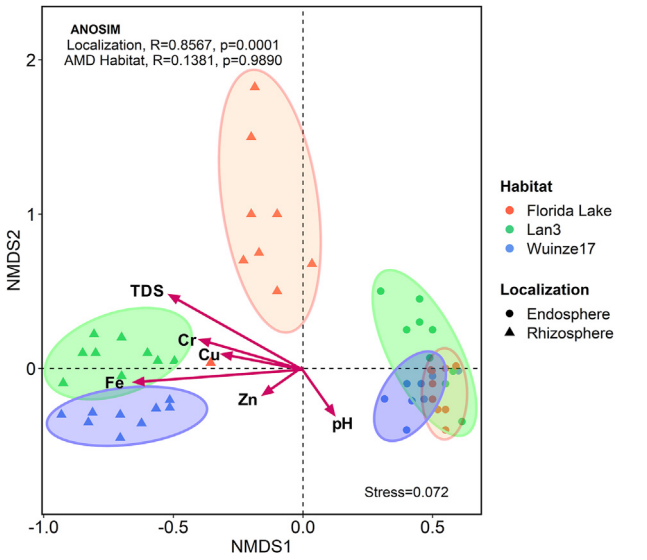

Figure 5. NMDS plots derived from Bray-Curtis similarity coefficient to show relationships among rhizosphere soil and root tissue primary metabolites in *Phragmites australis* growing in AMD contaminated wetland. Variables, including the habitat (AMD gradient) and localization (root endosphere vs rhizosphere), were added as community-influencing factors. *R* and *p*-values generated by ANOSIM test are shown at the upper part of the NMDS plot. Shaded ellipses represent confidence intervals around each sample population centroid. Vector fitting to the NMDS plot of the physicochemical environmental factors significantly associated ($p < 0.05$) with the ordination space as defined by the metabolite composition is presented by arrows.

two AMD sites. Consistent with these findings, other studies have also reported that increasing heavy metal levels greatly affects microbial communities in soils, leading to reduced microbial diversity, richness, and metabolic activity [38, 39, 40]. However, soil fungal communities are less affected by heavy metals compared to soil bacterial communities [39, 41]. Interestingly, fungal diversity was generally higher in the root endosphere than the rhizospheric samples (Table 2). Unlike our study, previous reports have suggested that microbial diversity and richness gradually decrease from the soil to the root-endosphere, with rhizosphere soil having higher diversity than the root endosphere. Generally, the assembly of the root microbial community has been postulated to occur in a two-step fashion. Whereas the rhizosphere is colonized by a subset of the bulk soil community, the rhizoplane and the endosphere are colonized by a subset of the rhizosphere community [11, 42]. For example, a study by Gottel *et al.* [43] reported that while endophytic bacteria richness in *Populus deltoides* under different soil types was highly variable and 10-fold lower than that of the rhizosphere, the fungal community diversity was not significantly different. Similarly, a strikingly higher OTU richness of fungal community has been reported in the rhizosphere than the endophytic compartments of poplar trees [44], and a subtropical island shrub *Mussaenda kwangtungensis* [45]. In these studies, it is postulated that the rhizosphere, generally characterized by presence of root exudates, mucilage produced by the root caps, and the release of sloughed-off root cells, is an active transition zone that provides suitable ecological niches for the growth, development, and reproduction of microbial communities [46]. On the other hand, environmental filters related to requirement for expression of genes associated with the production of cell-wall-degrading enzymes and resistance to a range of plant innate immune responses for successful endophytic compartment colonization, may account for the observed lower microbial diversity [44, 45, 47]. Collectively, the reported higher fungal diversity and richness of the aforementioned taxa may indicate that the local *P. australis* rhizospheric microenvironment has a complex effect on the fungal community, selecting for more endophytic metal tolerant groups under AMD-stress conditions. However, whether these observations could also be attributed to the inherent experimental challenge of low sample size used, varying copy numbers for the tandemly repeated nuclear ribosomal operon [48], PCR biases [49], and efficiency differences of DNA extraction from endophytic and rhizospheric compartment samples [50], also warrants further investigation.

In this study, *Ascomycota* and *Basidiomycota* were the dominant phyla (>% of high-quality sequences) across all AMD samples. Congruent to our findings, Baker *et al.* [51] also reported that members of the phylum *Ascomycota* and *Basidiomycota* primarily dominating the sub-surface low-pH biofilms in Richmond mine (Iron Mountain). At the class level, *Saccharomycetales*, *Eurotiomycetes*, *Tremellomycetes*, *Agraricomycetes*, *Microbotryomycetes_uc*, *Ustlaginomycetes*, *Dothideomycetes*, *Sordariomycetes*, *Leotiomycetes*, and *Cystobasidiomycetes* were the dominant groups. Interestingly, both rhizosphere and root endosphere in two AMD sites had significantly higher levels of phylum *Ascomycota* compared to non-AMD samples. As co-adaptation between plants and its rhizospheric soil microbiota is essential to cope with edaphic stresses under extreme environment, the observed higher abundance of members of phylum *Ascomycota* belonging to class *Dothideomycetes* and *Eurotiomycetes* imply they could be playing important roles in the ecology and stability of

Table 3. Major primary metabolites significantly associated with distinct root endosphere and rhizosphere of *Phragmites australis* growing under AMD-polluted environments.

Metabolites	Type	IndVal.g[a]		*p*-value
		Endosphere	Rhizosphere	
Adenosine	Nucleotide	0.862	-	0.0001
Acetylcholine	Signal molecule	0.665	-	0.0094
Symmetric dimethylarginine	Amino acid	0.636	-	0.0003
Asymmetric dimethylarginine	Amino acid	0.599	-	0.0015
Dopa	Other	0.595	-	0.0061
Guanosine monophosphate	Nucleotide	0.522	-	0.0032
Kynurenine	Others	0.488	-	0.0451
Isoleucine	Amino acid	0.451	-	0.0006
Leucine	Amino acid	0.381	-	0.0005
Niacinamide	Others		0.823	0.0001
Creatinine	Organic acid	-	0.661	0.0054
Ophthalmic acid	Organic acid	-	0.654	0.0001
2-Ketoglutaric acid	Organic acid	-	0.643	0.0088
Serotonin	Others	-	0.632	0.0105
Histamine	Others	-	0.611	0.0005
Guanosine	Nucleotide	-	0.608	0.0001
Methionine	Amino acid	-	0.602	0.0005
Dimethylglycine	Amino acid	-	0.573	0.0007
Thymidine monophosphate	Nucleotide	-	0.570	0.0103
Thymine	Nucleotide	-	0.568	0.0056
Choline	Others	-	0.556	0.0036
Cystathionine	Amino acid	-	0.533	0.0311
Proline	Amino acid	-	0.504	0.0314
Valine	Amino acid	-	0.435	0.0329

[a] The generalized indicator value (*IndVal.g*) and corresponding *p*-values used to assess the predictive value of a metabolite for either rhizosphere or endosphere as implemented in *indicspecies* in R [37] is given.

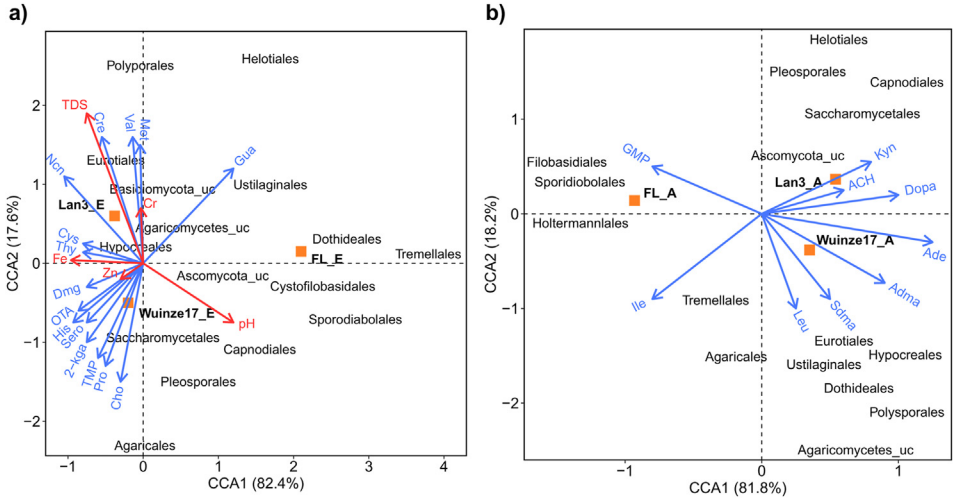

Figure 6. Canonical correspondence analysis (CCA) triplot results. (a) The relationships among the abundance of fungal genera, major primary metabolites of rhizosphere samples and the physiochemical parameters in *Phragmites australis* growing in different AMD contaminated environments. (b) Ordination of root endosphere fungal genera and primary metabolomes. The percentages on each axis represent the variation in samples. Blue and red vectors represent the direction of the variables that could explain sites ordination. Abbreviations for primary metabolites [*ACH*, acetylcholine; *Cre*, creatinine; *Sero*, serotonin; *Ade*, adenosine; *Adma*, asymmetric dimethylarginine; *IIe*, isoleucine; *His*, histamine; *GMP*, guanosine monophosphate; *Gua*, guanosine; *2-kga*, 2-ketoglutaric acid; *Cys*, cystathionine; *Pro*, proline; *Ota*, ophthalmic acid; *Dmg*, dimethylglycine; *Cho*, choline; *Tmp*, thymidine monophosphate; *Thy*, thymine; *Ncn*, niacinamide; *Orn*, ornithine; *Val*, valine; *Met*, methionine, and *Kyn*, Kynurenine].

P. australis under such extreme environment. Several studies have reported that filamentous fungal genera such as *Aspergillus*, *Mucor*, and *Trichoderma* [52, 53, 54], *Rhodotorula* [55], *Rhizopus* [56], and *Penicillium* [57] are adaptable to environmental heavy metal contamination, detoxify them through inherent mechanisms such as transformation, crystallization, extracellular precipitation, complexation, and cellular absorption [57, 58, 59]. In this study, members of genera *Penicillium*, *Candida*, *Saccharomycetales*, *Vishniacozyma*, *Trichoderma*, *Cladosporium*, and unclassified *Didymellaceae* were highly enriched in the root endosphere and rhizospheric samples from AMD sites compared to the non-AMD site (Figure 3c). Yamaji *et al.* [60] also reported the tolerance of *Clethra barbinervis* to heavy metal as impacted by root fungal endophytes.

Like ectomycorrhizal fungi, metal resistant root fungal endophytes utilize the enhancement of the antioxidative system, mediating heavy-metal distribution in plant cells and detoxification of heavy metal to induce tolerance of plants to heavy-metal stress [61]. Further, endo- and ectomycorrhizal fungi produce siderophores and enzymes important in the reduction of plant ethylene levels and thereby enhancing plant growth [60]. Thus, root fungal endophytes and ectophytes (*Ascomycota* and *Basidiomycota*) reported collectively may be contributing to the many

critical ecological functions including metal tolerance and detoxification, carbon, and nitrogen cycling [11, 60], important for the fidelity and proliferation of the reed plant within the extreme AMD environment.

4.2. Spatially defined root metabolome in P. australis is dependent on AMD gradient

Under conditions of heavy metal stress, plants have evolved numerous defense mechanisms ranging from reduced metal uptake, sequestration of metal into vacuoles, binding to phytochelatins/metallothioneins, activation of various antioxidants, to build-up of large quantities and diverse primary and secondary metabolites [62, 63]. These studies further reported that Cd, Cu, Ni, and Zn preferentially influence the production of nitrogen-containing metabolites. Several studies using different proteomic techniques such as 2-D electrophoresis, MALDI-TOF, LC-MS have also reported the involvement of target proteins and metabolites such as various amino acids, amines, organic acids, phenol, glutathione, and α-tocopherol in heavy metal stress tolerance and detoxification in several plants [64, 65, 66]. Additionally, the role of cyclic nucleotides, hydrogen ions, choline, signaling compounds such as acetylcholine (ACH) in heavy metal stress signal transduction has been reported [67]. In this study, spatially defined metabolite exudation by distinct root parts (rhizosphere *vs* endosphere) rather than AMD sites was observed (Figure 5, Table 3). Further, spatial separation in the NMDS ordination space was visible in rhizospheric compartment for the non-AMD site from AMD site. Plants generally attempts to have homeostatic control on the internal root environment even under stressful conditions, and this may explain no significant observed difference in the primary metabolites' exudation in the root endospheric compartments compared to the environmentally exposed rhizosphere in AMD and non-AMD sites. However, it should be noted that the type and amount plant exudation is dependent on several factors such as plant genotype, metabolite class produced and abiotic stress [11, 68].

Comparatively, the AMD sites induced the production of more primary metabolites in the root rhizosphere than endosphere of *P. australis* (Table 3, Figure 6a). These metabolites included amino acids (proline, methionine, valine, cystathionine, and dimethylglycine), organic acids (2-ketoglutaric acid, creatinine, and ophthalmic acid), nucleotides (thymine and thymidine monophosphate) and amines and other signaling compounds (choline, serotonin, niacinamide, and histamine). Work done by several researchers have also reported that under heavy metal stress, elevated production of methionine and niacinamide plays important role in the signaling, sequestration, and transportation of heavy metals such as Fe, Cu, Zn, Cd [67, 69, 70, 71, 72]. Furthermore, the role of root exudates in enhancing mobility of metals and nutrients via acidification due to proton (H^+) release or by forming organic/amino acid-metal/mineral complexes have been reported [12, 15]. The AMD sites were characterized by 2-10-fold higher heavy metal content (Fe, Cr, Cu, and Zn) (Table 1), which correlated with observed higher production of methionine and niacinamide compared to the non-AMD site (Figure 4, Figure 6a). Additionally, choline, ophthalmic acid, and proline were positively and significantly associated with the rhizospheric samples in AMD sites (Figure 6a). Whereas ophthalmic acid is a marker of oxidative stress in plants, the up-regulation of proline in plants and microorganisms is an indication of heavy metal stress [73, 74, 75]. Proline is also known for its ability to function as an osmolyte, radical scavenger, electron sink, stabilizer of macromolecules, and a cell wall component, and its accumulation is generally induced dependent heavy metal type and concentration [70]. Consistent with current findings, heavy metal treatment has been associated with higher organic acid exudation in poplar (*Populus tremula*) [76]. Furthermore, the exudation of organic acid anions (malate, citrate and oxalate) change the redox state and pH of soil are important for mobilization of inorganic phosphorous from P-deprived soils and chelation to improve Al toxicity in acidic soils [77]. On the other hand, intermediary metabolite choline that can be synthesized exogenously by both plants and fungi has been reported to promote the fungal growth and enhance their survival in stressed environments [78, 79]. Current results, therefore, corroborate the assertions that the production of these metabolites is one of the key adaptive mechanisms by *P. australis* to overcome heavy metal and low pH stress in the AMD setting.

By applying CCA, we detected that rhizospheric fungal taxonomic changes observed across the AMD sites were driven by a combination of pH, TDS, EC, and primary metabolites. Specifically, members of *Polyporales*, *Eurotiales*, and *Hypocreales* had a significant and positive correlation with the physicochemical parameters (EC and TDS) in the rhizosphere of the AMD site Lan 3 (Figure 6a). In contrast, only pH exhibited a significant negative correlation with the fungal community at Lan 3. A study by Lauber *et al.* [80] and Mandakovic *et al.* [81] have previously reported that bacterial diversity in edaphic environments is unimodally correlated to pH, generally reaching a peak at near-neutral conditions and decreasing towards more acidic and more alkaline conditions. On the other hand, fungal communities have been reported to be less sensitive to soil pH variations [41], which is inconsistent with the current findings. However, low pH is generally associated with high bioavailability and toxicity of heavy metals [82, 83]. This may explain the lower fungal diversity observed under high AMD pollution conditions. Under mild AMD conditions (site Wuinze 17), the impact of primary metabolites on rhizospheric fungal diversity was more discernible, with dimethylglycine, ophthalmic acid, histamine, serotonin, 2-ketoglutaric acid, thymidine monophosphate, proline, and choline levels being significantly associated with members of the order *Agaricales* and *Saccharomycetales*. NMDS analysis also showed higher variability between such metabolites in the rhizosphere of the *P. australis* reed than the root tissues under AMD-polluted. This may imply that the production of metabolites and the fungal communities present in the acid mine drainage sites at the rhizospheric level are more environmentally dependent than in the root tissues. It is worth noting that rhizosphere microbiota may also play significant role in the differential root exudation profile, in addition to producing some of these metabolites on their own in order to increase their fidelity in the rhizospheric environment. For example, the role of microbiome-reprogrammed systemic root exudation in promoting soil conditioning has been reported in tomatoes [84]. In our study, we focused only on primary metabolome, which were all assumed to be of plant origin. Since, plant root exudation is a dynamic process, involving diverse primary and secondary metabolites likely dependent on a plethora or transporters that are mostly uncharacterized [11, 85], result of this study has only scratched the surface of *P. australis* metabolic diversity and rhizomicrobiome assembly. It is anticipated that further studies will continue to advance the mechanistic understanding of plant-microbe-heavy metal interactions in this important pseudometallophyte.

5. Conclusions

Overall, the results of this study indicate that spatially defined exudation as modulated by abiotic factors plays a key role in the rhizobiome assembly with the establishment of distinct fungal communities that were observed to be associated with specific root parts of *P. australis*. It is plausible that these interactions (between root exudates and fungal community in the rhizosphere) are a critical component of *P. australis* growth and adaptability to the heavy metal-laden and low pH AMD ecological niche. While the fungal community may be important in the metal mobilization, transformation, and detoxification leading to the plant heavy metal tolerance and remediation, they are also greatly influenced by the plant root exudates, that enrich the rhizosphere in nutrients, including acting as messengers to initiate interaction between plant and the beneficial microbiomes. However, it is worth noting that the synergistic action of plant and microbes and their mechanism for metal phytorhizoremediation under the AMD environment may involve a complex interaction involving numerous cryptic crosstalk and regulatory networks that are still largely unknown. The success of microbial colonization of the rhizosphere is also dependent on several factors, such as

chemotaxis, substrate specificity, competitiveness, and cooperativeness, whose understanding is currently limited. Further, plant root exudation is a dynamic process, involving diverse primary and secondary metabolites likely dependent on a plethora or transporters that are mostly uncharacterized [11, 85]. Nevertheless, the results of this study represent the first report that has attempted to delineate the importance of primary metabolites-fungal community-heavy metal interaction in the adaptability of *P. australis* under AMD environment. The beneficial effects exhibited by fungal groups reported related to heavy metal tolerance, as perturbed by *P. australis* root exudates and edaphic factors, illustrates their potential exploitation in the remediation of metal-contaminated environments. Future studies involving a large repertoire of spatial, temporal and biogeochemical factors, therefore, are needed to characterize the spatially distinct rhizobiomes (bacteria, fungi and archaea) and their functional traits, and at investigating spatially distinct root exudation (both primary and secondary metabolites) for deeper understanding of the intricate interactions between metallophytes and microbiomes in AMD environments.

Declarations

Author contribution statement

Chimdi Mang Kalu: Conceived and designed the experiments; Performed the experiments; Wrote the paper.

Henry Joseph Oduor Ogola: Performed the experiments; Analyzed and interpreted the data; Wrote the paper.

Ramganesh Selverajan: Performed the experiments; Analyzed and interpreted the data.

Memory Tekere: Contributed reagents, materials, analysis tools or data.

Khayalethu Ntushelo: Conceived and designed the experiments; Contributed reagents, materials, analysis tools or data.

Funding statement

This work was supported by the National Research Foundation of South Africa (grant number: 129095).

Data availability statement

Data associated with this study has been deposited at the NCBI database (https://www.ncbi.nlm.nih.gov/) sequence archive (SRA) as BioProject ID PRJNA640287.

Declaration of interests statement

The authors declare no conflict of interest.

Additional information

Supplementary content related to this article has been published online at https://doi.org/10.1016/j.heliyon.2021.e06399.

Acknowledgements

We thank the managers of the Jo'burg Parks, Mintails Mogale Gold Mine and Sibanye Gold Mine for granting permission to collect samples for the study.

References

[1] A. RoyChowdhury, D. Sarkar, R. Datta, Remediation of acid mine drainage-impacted water, Curr. Pollut. Rep. 1 (2015) 131–141.
[2] P.K. Das, Phytoremediation and nanoremediation: emerging techniques for treatment of acid mine drainage water, Def Life Sci J. 3 (2018) 190–196.
[3] R.H. Kadlec, S. Wallace, Treatment Wetlands, CRC press, 2008.
[4] H. Brix, C.A. Arias, N.H. Johansen, Experiments in a two-stage constructed wetland system: nitrification capacity and effects of recycling on nitrogen removal, in: Wetl. Met. Mass Cycl., 2003, pp. 237–258.
[5] J. Vymazal, L. Krőpfelová, Growth of Phragmites australis and Phalaris arundinacea in constructed wetlands for wastewater treatment in the Czech Republic, Ecol. Eng. 25 (2005) 606–621.
[6] R. Wang, N. Korboulewsky, P. Prudent, M. Domeizel, C. Rolando, G. Bonin, Feasibility of using an organic substrate in a wetland system treating sewage sludge: impact of plant species, Bioresour. Technol. 101 (2010) 51–57.
[7] A. San Miguel, P. Ravanel, M. Raveton, A comparative study on the uptake and translocation of organochlorines by Phragmites australis, J. Hazard Mater. 244 (2013) 60–69.
[8] K.K. Chiu, Z.H. Ye, M.H. Wong, Growth of Vetiveria zizanioides and Phragmities australis on Pb/Zn and Cu mine tailings amended with manure compost and sewage sludge: a greenhouse study, Bioresour. Technol. 97 (2006) 158–170.
[9] C. Mant, S. Costa, J. Williams, E. Tambourgi, Phytoremediation of chromium by model constructed wetland, Bioresour. Technol. 97 (2006) 1767–1772.
[10] T. Toyama, T. Furukawa, N. Maeda, D. Inoue, K. Sei, K. Mori, S. Kikuchi, M. Ike, Accelerated biodegradation of pyrene and benzo [a] pyrene in the Phragmites australis rhizosphere by bacteria–root exudate interactions, Water Res. 45 (2011) 1629–1638.
[11] J. Sasse, E. Martinoia, T. Northen, Feed your friends: do plant exudates shape the root microbiome? Trends Plant Sci. 23 (2018) 25–41.
[12] Y. Ma, R.S. Oliveira, H. Freitas, C. Zhang, Biochemical and molecular mechanisms of plant-microbe-metal interactions: relevance for phytoremediation, Front. Plant Sci. 7 (2016) 918. https://www.frontiersin.org/article/10.3389/fpls.2016.00918.
[13] S. Borymski, M. Cycoń, M. Beckmann, L.A.J. Mur, Z. Piotrowska-Seget, Plant species and heavy metals affect biodiversity of microbial communities associated with metal-tolerant plants in metalliferous soils, Front. Microbiol. 9 (2018) 1425.
[14] W. Zhang, Z. Huang, L. He, X. Sheng, Assessment of bacterial communities and characterization of lead-resistant bacteria in the rhizosphere soils of metal-tolerant Chenopodium ambrosioides grown on lead–zinc mine tailings, Chemosphere 87 (2012) 1171–1178.
[15] A. Sessitsch, M. Kuffner, P. Kidd, J. Vangronsveld, W.W. Wenzel, K. Fallmann, M. Puschenreiter, The role of plant-associated bacteria in the mobilization and phytoextraction of trace elements in contaminated soils, Soil Biol. Biochem. 60 (2013) 182–194.
[16] D.K. DeForest, K.V. Brix, W.J. Adams, Assessing metal bioaccumulation in aquatic environments: the inverse relationship between bioaccumulation factors, trophic transfer factors and exposure concentration, Aquat. Toxicol. 84 (2007) 236–246.
[17] P. Angelini, A. Rubini, D. Gigante, L. Reale, R. Pagiotti, R. Venanzoni, The endophytic fungal communities associated with the leaves and roots of the common reed (Phragmites australis) in Lake Trasimeno (Perugia, Italy) in declining and healthy stands, Fungal Ecol. 5 (2012) 683–693.
[18] M.S. Fischer, R.J. Rodriguez, Fungal endophytes of invasive Phagramites australis populations vary in species composition and fungicide susceptibility, Symbiosis 61 (2013) 55–62.
[19] K.P. Kowalski, C. Bacon, W. Bickford, H. Braun, K. Clay, M. Leduc-Lapierre, E. Lillard, M.K. McCormick, E. Nelson, M. Torres, J. White, D.A. Wilcox, Advancing the science of microbial symbiosis to support invasive species management: a case study on Phragmites in the Great Lakes, Front. Microbiol. 6 (2015) 95. https://www.frontiersin.org/article/10.3389/fmicb.2015.00095.
[20] N. Dolinar, A. Gaberščik, Mycorrhizal colonization and growth of Phragmites australis in an intermittent wetland, Aquat. Bot. 93 (2010) 93–98.
[21] J. Ludwig-Müller, Plants and endophytes: equal partners in secondary metabolite production? Biotechnol. Lett. 37 (2015) 1325–1334.
[22] K. Yamamoto, Y. Shiwa, T. Ishige, H. Sakamoto, K. Tanaka, M. Uchino, N. Tanaka, S. Oguri, H. Saitoh, S. Tsushima, Bacterial diversity associated with the rhizosphere and endosphere of two halophytes: glaux maritima and Salicornia europaea, Front. Microbiol. 9 (2018) 2878.
[23] L. Sekhohola-Dlamini, R. Selvarajan, H.J.O. Ogola, M. Tekere, Community diversity metrics, interactions, and metabolic functions of bacteria associated with municipal solid waste landfills at different maturation stages, n/a, Microbiologyopen (2020) e1118.
[24] C. Chen, S.S. Khaleel, H. Huang, C.H. Wu, Software for pre-processing Illumina next-generation sequencing short read sequences, Source Code Biol. Med. 9 (2014) 1–11.
[25] T. Magoč, S.L. Salzberg, FLASH: fast length adjustment of short reads to improve genome assemblies, Bioinformatics 27 (2011) 2957–2963.
[26] N.A. Bokulich, S. Subramanian, J.J. Faith, D. Gevers, J.I. Gordon, R. Knight, D.A. Mills, J.G. Caporaso, Quality-filtering vastly improves diversity estimates from Illumina amplicon sequencing, Nat. Methods 10 (2013) 57–59.
[27] E. Bolyen, J.R. Rideout, M.R. Dillon, N.A. Bokulich, C.C. Abnet, G.A. Al-Ghalith, H. Alexander, E.J. Alm, M. Arumugam, F. Asnicar, Reproducible, interactive, scalable and extensible microbiome data science using QIIME 2, Nat. Biotechnol. 37 (2019) 852–857.
[28] R. Edgar, UCHIME2: improved chimera prediction for amplicon sequencing, BioRxiv (2016), 074252.
[29] R.C. Edgar, UPARSE: highly accurate OTU sequences from microbial amplicon reads, Nat. Methods 10 (2013) 996.
[30] Q. Wang, G.M. Garrity, J.M. Tiedje, J.R. Cole, Native Bayesian classifier for rapid assignment of rRNA sequences into the new bacterial taxonomy, Appl. Environ. Microbiol. 73 (2007) 5261–5267.
[31] P.J. McMurdie, S. Holmes, Phyloseq: an R package for reproducible interactive analysis and graphics of microbiome census data, PloS One 8 (2013), e61217.

[32] K.S. Andersen, R.H. Kirkegaard, S.M. Karst, M. Albertsen, ampvis2: an R package to analyse and visualise 16S rRNA amplicon data, BioRxiv (2018) 299537.
[33] O. Hammer, D.A.T. Harper, P.D. Ryan, Palaeontological statistics software package for education and data analysis, Palaeontol. Electron. 4 (2001).
[34] H. Wickham, ggplot2: Elegant Graphics for Data Analysis, Springer, 2016.
[35] G.R. Warnes, B. Bolker, L. Bonebakker, R. Gentleman, W.H.A. Liaw, T. Lumley, gplots: various R programming tools for plotting data, R package version 3.0. 1.1. 2019, 2019.
[36] J. Oksanen, F.G. Blanchet, R. Kindt, P. Legendre, R.B. O'hara, G.L. Simpson, P. Solymos, M.H.H. Stevens, H. Wagner, Vegan: community ecology package. R package version 1.17-4, 2010. URL, http//cran. r-project.org/package=vegan.
[37] M. De Cáceres, P. Legendre, M. Moretti, Improving indicator species analysis by combining groups of sites, Oikos 119 (2010) 1674–1684.
[38] X.-Y. Zeng, S.-W. Li, Y. Leng, X.-H. Kang, Structural and functional responses of bacterial and fungal communities to multiple heavy metal exposure in arid loess, Sci. Total Environ. (2020) 138081.
[39] A. Frossard, M. Hartmann, B. Frey, Tolerance of the forest soil microbiome to increasing mercury concentrations, Soil Biol. Biochem. 105 (2017) 162–176.
[40] J. Edwards, C. Johnson, C. Santos-Medellín, E. Lurie, N.K. Podishetty, S. Bhatnagar, J.A. Eisen, V. Sundaresan, Structure, variation, and assembly of the root-associated microbiomes of rice, Proc. Natl. Acad. Sci. 112 (2015) E911–E920.
[41] L. Deng, G. Zeng, C. Fan, L. Lu, X. Chen, M. Chen, H. Wu, X. He, Y. He, Response of rhizosphere microbial community structure and diversity to heavy metal co-pollution in arable soil, Appl. Microbiol. Biotechnol. 99 (2015) 8259–8269.
[42] D. Bulgarelli, K. Schlaeppi, S. Spaepen, E.V.L. van Themaat, P. Schulze-Lefert, Structure and functions of the bacterial microbiota of plants, Annu. Rev. Plant Biol. 64 (2013) 807–838.
[43] N.R. Gottel, H.F. Castro, M. Kerley, Z. Yang, D.A. Pelletier, M. Podar, T. Karpinets, E.D. Uberbacher, G.A. Tuskan, R. Vilgalys, Distinct microbial communities within the endosphere and rhizosphere of Populus deltoides roots across contrasting soil types, Appl. Environ. Microbiol. 77 (2011) 5934–5944.
[44] B. Beckers, M.O. De Beeck, N. Weyens, W. Boerjan, J. Vangronsveld, Structural variability and niche differentiation in the rhizosphere and endosphere bacterial microbiome of field-grown poplar trees, Microbiome 5 (2017) 1–17.
[45] X. Qian, H. Li, Y. Wang, B. Wu, M. Wu, L. Chen, X. Li, Y. Zhang, X. Wang, M. Shi, Y. Zheng, L. Guo, D. Zhang, Leaf and root endospheres harbor lower fungal diversity and less complex fungal Co-occurrence patterns than rhizosphere, Front. Microbiol. 10 (2019) 1015. https://www.frontiersin.org/article/10.3389/fmicb.2019.01015.
[46] J.M. Raaijmakers, The minimal rhizosphere microbiome. Princ. Plant-Microbe Interact., Springer, 2015, pp. 411–417.
[47] P.R. Hardoim, L.S. van Overbeek, J.D. van Elsas, Properties of bacterial endophytes and their proposed role in plant growth, Trends Microbiol. 16 (2008) 463–471.
[48] A.R.D. Ganley, T. Kobayashi, Highly efficient concerted evolution in the ribosomal DNA repeats: total rDNA repeat variation revealed by whole-genome shotgun sequence data, Genome Res. 17 (2007) 184–191.
[49] R. Sipos, A.J. Székely, M. Palatinszky, S. Révész, K. Márialigeti, M. Nikolausz, Effect of primer mismatch, annealing temperature and PCR cycle number on 16S rRNA gene-targetting bacterial community analysis, FEMS Microbiol. Ecol. 60 (2007) 341–350.
[50] A.S. Amend, K.A. Seifert, T.D. Bruns, Quantifying microbial communities with 454 pyrosequencing: does read abundance count? Mol. Ecol. 19 (2010) 5555–5565.
[51] B.J. Baker, G.W. Tyson, L. Goosherst, J.F. Banfield, Insights into the diversity of eukaryotes in acid mine drainage biofilm communities, Appl. Environ. Microbiol. 75 (2009) 2192–2199.
[52] I. Acosta-Rodríguez, J.F. Cárdenas-González, A.S. Rodríguez Pérez, J.T. Oviedo, V.M. Martínez-Juárez, Bioremoval of different heavy metals by the resistant fungal strain Aspergillus Niger, Bioinorgan. Chem. Appl. 2018 (2018).
[53] J. Yang, Q. Wang, Q. Luo, Q. Wang, T. Wu, Biosorption behavior of heavy metals in bioleaching process of MSWI fly ash by Aspergillus Niger, Biochem. Eng. J. 46 (2009) 294–299.
[54] O.G. Oladipo, O.O. Awotoye, A. Olayinka, C.C. Bezuidenhout, M.S. Maboeta, Heavy metal tolerance traits of filamentous fungi isolated from gold and gemstone mining sites, Braz. J. Microbiol. 49 (2018) 29–37.
[55] S. Grujić, S. Vasić, I. Radojević, L. Čomić, A. Ostojić, Comparison of the Rhodotorula mucilaginosa biofilm and planktonic culture on heavy metal susceptibility and removal potential, Water, Air, Soil Pollut. 228 (2017) 73.
[56] E.M. Fawzy, F.F. Abdel-Motaal, S.A. El-zayat, Biosorption of heavy metals onto different eco-friendly substrates, J. Toxicol. Environ. Health Sci. 9 (2017) 35–44.
[57] L.B. Glukhova, Y.A. Frank, E. V Danilova, M.R. Avakyan, D. Banks, O.H. Tuovinen, O. V Karnachuk, Isolation, characterization, and metal response of novel, acid-tolerant Penicillium spp. from extremely metal-rich waters at a mining site in Transbaikal (Siberia, Russia), Microb. Ecol. 76 (2018) 911–924.
[58] A. Bankar, S. Zinjarde, M. Shinde, G. Gopalghare, A. Ravikumar, Heavy metal tolerance in marine strains of Yarrowia lipolytica, Extremophiles 22 (2018) 617–628.
[59] J.A. Sayer, M. Kierans, G.M. Gadd, Solubilisation of some naturally occurring metal-bearing minerals, limescale and lead phosphate by Aspergillus Niger, FEMS Microbiol. Lett. 154 (1997) 29–35.
[60] K. Yamaji, Y. Watanabe, H. Masuya, A. Shigeto, H. Yui, T. Haruma, Root fungal endophytes enhance heavy-metal stress tolerance of Clethra barbinervis growing naturally at mining sites via growth enhancement, promotion of nutrient uptake and decrease of heavy-metal concentration, PloS One 11 (2016).
[61] X. Li, W. Li, L. Chu, J.F. White, Z. Xiong, H. Li, Diversity and heavy metal tolerance of endophytic fungi from Dysphania ambrosioides, a hyperaccumulator from Pb–Zn contaminated soils, J. Plant Interact. 11 (2016) 186–192.
[62] S. Tiwari, C. Lata, Heavy metal stress, signaling, and tolerance due to plant-associated microbes: an overview, Front. Plant Sci. 9 (2018) 452.
[63] M. Shahid, S. Khalid, G. Abbas, N. Shahid, M. Nadeem, M. Sabir, M. Aslam, C. Dumat, Heavy metal stress and crop productivity, in: Crop Prod. Glob. Environ. Issues, Springer, 2015, pp. 1–25.
[64] D. Kısa, M. Elmastaş, L. Öztürk, Ö. Kayır, Responses of the phenolic compounds of Zea mays under heavy metal stress, Appl. Biol. Chem. 59 (2016) 813–820.
[65] R. Wang, F. Gao, B.-Q. Guo, J.-C. Huang, L. Wang, Y.-J. Zhou, Short-term chromium-stress-induced alterations in the maize leaf proteome, Int. J. Mol. Sci. 14 (2013) 11125–11144.
[66] S. Singh, P. Parihar, R. Singh, V.P. Singh, S.M. Prasad, Heavy metal tolerance in plants: role of transcriptomics, proteomics, metabolomics, and ionomics, Front. Plant Sci. 6 (2016) 1143.
[67] S.K. Jalmi, P.K. Bhagat, D. Verma, S. Noryang, S. Tayyeba, K. Singh, D. Sharma, A.K. Sinha, Traversing the links between heavy metal stress and plant signaling, Front. Plant Sci. 9 (2018) 12.
[68] U.G. Mueller, J.L. Sachs, Engineering microbiomes to improve plant and animal health, Trends Microbiol. 23 (2015) 606–617.
[69] X. Zhou, S. Li, Q. Zhao, X. Liu, S. Zhang, C. Sun, Y. Fan, C. Zhang, R. Chen, Genome-wide identification, classification and expression profiling of nicotianamine synthase (NAS) gene family in maize, BMC Genom. 14 (2013) 238.
[70] G. Yang, J. Li, W. Liu, Z. Yu, Y. Shi, B. Lv, B. Wang, D. Han, Molecular cloning and characterization of MxNAS2, a gene encoding nicotianamine synthase in Malus xiaojinensis, with functions in tolerance to iron stress and misshapen flower in transgenic tobacco, Sci. Hortic. (Amsterdam) 183 (2015) 77–86.
[71] M. Safdarian, H. Askari, V. Shariati, G. Nematzadeh, Transcriptional responses of wheat roots inoculated with Arthrobacter nitroguajacolicus to salt stress, Sci. Rep. 9 (2019) 1–12.
[72] A.A.T. Johnson, B. Kyriacou, D.L. Callahan, L. Carruthers, J. Stangoulis, E. Lombi, M. Tester, Constitutive overexpression of the OsNAS gene family reveals single-gene strategies for effective iron-and zinc-biofortification of rice endosperm, PloS One 6 (2011).
[73] S.S. Sharma, K.-J. Dietz, The significance of amino acids and amino acid-derived molecules in plant responses and adaptation to heavy metal stress, J. Exp. Bot. 57 (2006) 711–726.
[74] C.T. Chen, L.-M. Chen, C.C. Lin, C.H. Kao, Regulation of proline accumulation in detached rice leaves exposed to excess copper, Plant Sci. 160 (2001) 283–290.
[75] B.N. Tripathi, J.P. Gaur, Relationship between copper-and zinc-induced oxidative stress and proline accumulation in Scenedesmus sp, Planta 219 (2004) 397–404.
[76] R. Qin, Y. Hirano, I. Brunner, Exudation of organic acid anions from poplar roots after exposure to Al, Cu and Zn, Tree Physiol. 27 (2007) 313–320.
[77] Z.C. Chen, H. Liao, Organic acid anions: an effective defensive weapon for plants against aluminum toxicity and phosphorus deficiency in acidic soils, J. Genet. Genom. 43 (2016) 631–638.
[78] Y.-I. Park, J.E. Gander, Choline derivatives involved in osmotolerance of Penicillium fellutanum, Appl. Environ. Microbiol. 64 (1998) 273–278.
[79] K. Lambou, A. Pennati, I. Valsecchi, R. Tada, S. Sherman, H. Sato, R. Beau, G. Gadda, J.-P. Latgé, Pathway of glycine betaine biosynthesis in Aspergillus fumigatus, Eukaryot. Cell 12 (2013) 853–863.
[80] C.L. Lauber, M. Hamady, R. Knight, N. Fierer, Pyrosequencing-based assessment of soil pH as a predictor of soil bacterial community structure at the continental scale, Appl. Environ. Microbiol. 75 (2009) 5111–5120.
[81] D. Mandakovic, J. Maldonado, R. Pulgar, P. Cabrera, A. Gaete, V. Urtuvia, M. Seeger, V. Cambiazo, M. González, Microbiome analysis and bacterial isolation from Lejía lake soil in Atacama desert, Extremophiles 22 (2018) 665–673.
[82] A.R. Schneider, M. Gommeaux, J. Duclercq, N. Fanin, A. Conreux, A. Alahmad, J. Lacoux, D. Roger, F. Spicher, M. Ponthieu, Response of bacterial communities to Pb smelter pollution in contrasting soils, Sci. Total Environ. 605 (2017) 436–444.
[83] J. Rousk, E. Bååth, P.C. Brookes, C.L. Lauber, C. Lozupone, J.G. Caporaso, R. Knight, N. Fierer, Soil bacterial and fungal communities across a pH gradient in an arable soil, ISME J. 4 (2010) 1340–1351.
[84] E. Korenblum, Y. Dong, J. Szymanski, S. Panda, A. Jozwiak, H. Massalha, S. Meir, I. Rogachev, A. Aharoni, Rhizosphere microbiome mediates systemic root metabolite exudation by root-to-root signaling, Proc. Natl. Acad. Sci. 117 (2020) 3874–3883.
[85] H. Liu, L.E. Brettell, Z. Qiu, B.K. Singh, Microbiome-mediated stress resistance in plants, Trends Plant Sci. 25 (2020) 733–743.